AFRL-OSR-VA-TR-2014-0065

PLASTICITY IN HIGH TEMPERATURE MATERIALS: TANTALUM AND MONAZITE

Jeffrey Kysar
THE TRUSTEES OF COLUMBIA UNIVERSITY IN THE CITY OF NEW YORK INC NEW YORK NY

03/12/2014
Final Report

Air Force Research Laboratory
AF Office Of Scientific Research (AFOSR)/ RTD
Arlington, Virginia 22203
Air Force Materiel Command

REPORT DOCUMENTATION PAGE

Form Approved
OMB No. 0704-0188

1. REPORT DATE *(DD-MM-YYYY)*	**2. REPORT TYPE**	**3. DATES COVERED** *(From - To)*
28-02-2014	FINAL	15 Feb 2009 - 30 Nov 2013

4. TITLE AND SUBTITLE

Plasticity in High Temperature Materials: Tantalum and Monazite

5a. CONTRACT NUMBER
N/A

5b. GRANT NUMBER
FA9550-09-1-0048

5c. PROGRAM ELEMENT NUMBER
FA9550

6. AUTHOR(S)
Prof. Jeffrey W. Kysar

5d. PROJECT NUMBER
GG001703

5e. TASK NUMBER

5f. WORK UNIT NUMBER
N/A

7. PERFORMING ORGANIZATION NAME(S) AND ADDRESS(ES)
THE TRUSTEES OF COLUMBIA UNIVERSITY IN THE CITY OF NEW
SPONSORED PROJECTS ADMINISTRATION
615 WEST 131 STREET, ROOM 254, MC
NEW YORK, NY 10027-6900

8. PERFORMING ORGANIZATION REPORT NUMBER
GG001703

9. SPONSORING / MONITORING AGENCY NAME(S) AND ADDRESS(ES)
USAF, AFRL DUNS 143574726
AF OFFICE OF SCIENTIFIC RESEARCH
875 N. RANDOLPH ST. ROOM 3112
ARLINGTON VA 22203
MATTHEW L. CIFA (703) 835-3577 / matthew.cifa@afosr.af.mil

10. SPONSOR/MONITOR'S ACRONYM(S)
AFOSR/PKR

11. SPONSOR/MONITOR'S REPORT NUMBER(S)

12. DISTRIBUTION / AVAILABILITY STATEMENT

13. SUPPLEMENTARY NOTES

14. ABSTRACT

The mechanical response materials under extreme conditions is of fundamental interest both for the fabrication of components for high-performance systems as well as the reliability of components once they are deployed in service. Dislocation-mediated plastic deformation is one of the most industrially significant deformation mechanisms yet a predictive and experimentally-validated understanding of plastic deformation in materials remains elusive due to the multiple length and time scales over which various phenomena occur. Traditionally scientists and engineers take either a "top-down" or a "bottom-up" approach across the length scales, but a significant gap remains in our understanding of how the smaller length scale phenomena interact with the larger length scale phenomena across the mesoscale on the order of micrometers. In this study, the PI developed a multiple length scale experimental program that spans from a 20 nanometer to a 3 micrometer spatial resolution, thus bridging the mesoscale. For face-centered cubic nickel, the methodology uncovered a scaling relationship between the dislocation mean free path length and GND density. For body-centered cubic tantalum, the methodology demonstrates a similar relationship.

15. SUBJECT TERMS

Geometrically Necessary Dislocation (GND) Density, Dislocation Mean Free Path Length, High Resolution Electron Backscatter

16. SECURITY CLASSIFICATION OF:			**17. LIMITATION OF ABSTRACT**	**18. NUMBER OF PAGES**	**19a. NAME OF RESPONSIBLE PERSON**
a. REPORT	**b. ABSTRACT**	**c. THIS PAGE**	UU	17	Xiomara Perez-Betances, AOR
U	U	U			**19b. TELEPHONE NUMBER** *(include area code)* 212-854-6851

Final Performance Report

Award Number

FA9550-09-1-0048

Funding Agency

Air Force Office of Scientific Research

Title of Project

Plasticity in High Temperature Materials: Tantalum and Monazite

February 28, 2014

Principal Investigator

Jeffrey W. Kysar
Professor of Mechanical Engineering
Department of Mechanical Engineering
Columbia University
244 Mudd Building, Mail Code 4703
500 W. 120th Street
New York, NY 10027

Executive Summary

The mechanical response materials—especially metals—under extreme conditions is of fundamental interest both for the fabrication of components for high-performance systems as well as the reliability of components once they are deployed in service. Dislocation-mediated plastic deformation is one of the most industrially significant deformation mechanisms yet a predictive and experimentally-validated understanding of plastic deformation in materials remains elusive due to the multiple length and time scales over which various phenomena occur. Traditionally scientists and engineers take either a "top-down" or a "bottom-up" approach across the length scales, but a significant gap remains in our understanding of how the smaller length scale phenomena interact with the larger length scale phenomena across the mesoscale on the order of micrometers. In this study, the PI has developed a multiple length scale experimental program that spans more than two orders of magnitude—from a 20 nanometer spatial resolution to a 3 micrometer spatial resolution—spanning the mesoscale. The rigorous lower bound of the Geometrically Necessary Dislocation (GND) density is measured using High Resolution Electron Backscatter Diffraction (HR-EBSD). When applied to face-centered cubic nickel, the methodology uncovered a scaling relationship between the dislocation mean free path length and GND density. When applied to body-centered cubic tantalum, the methodology also demonstrated a relationship between dislocation mean free path length and GND density. A framework to apply the methodology to monoclinic monazite was also developed.

The PI was the recipient of several awards during the period of this grant, including a best poster award, the International Journal of Plasticity Young Researcher Award, and was a lead author of the "Hot Paper in Chemistry" as reported by Science Watch during March-June 2010 as "the most-cited chemistry report published in the last two years, excluding reviews" for a study that acknowledged funding from a prior AFOSR grant.

Experimental Methodology

The goal of the experiments is to measure the spatial variation of the Geometrically Necessary Dislocation (GND) density over multiple length scales ranging from 20 nm to 3 μm in a single crystal specimen under plane strain conditions. Fig. 1a demonstrates the geometrical configuration of a face-centered cubic (FCC) specimen with plastic slip systems $\{111\}\langle 110\rangle$ oriented and loaded such that the (110) plane experiences plane strain deformation (full details in [1]). Upon application of a distributed line loading parallel to [110] on the (001) plane as shown in Fig. 1b for the case of a wedge indenter used in this project, the crystal lattice rotation that accompanies the plastic deformation occurs (ideally, in theory, and predominantly, in practice) only about the [110] axis. We refer to this as the in-plane lattice rotation, ω_3, as illustrated in Fig. 1c.

As discussed in [1], the plastic deformation induced in the crystal can be thought of as occurring due to three effective in-plane slip systems induced by cooperative slip on a pair or set of slip systems. Two of the effective slip systems are due to coplanar slip system pairs and the third is due to a collinear slip pair. All the dislocation junctions that form in an FCC crystal form as a consequence of plastic deformation are formed by different combinations of the slip system pairs (e.g. effective in-plane slip systems). Hence, while the deformation state

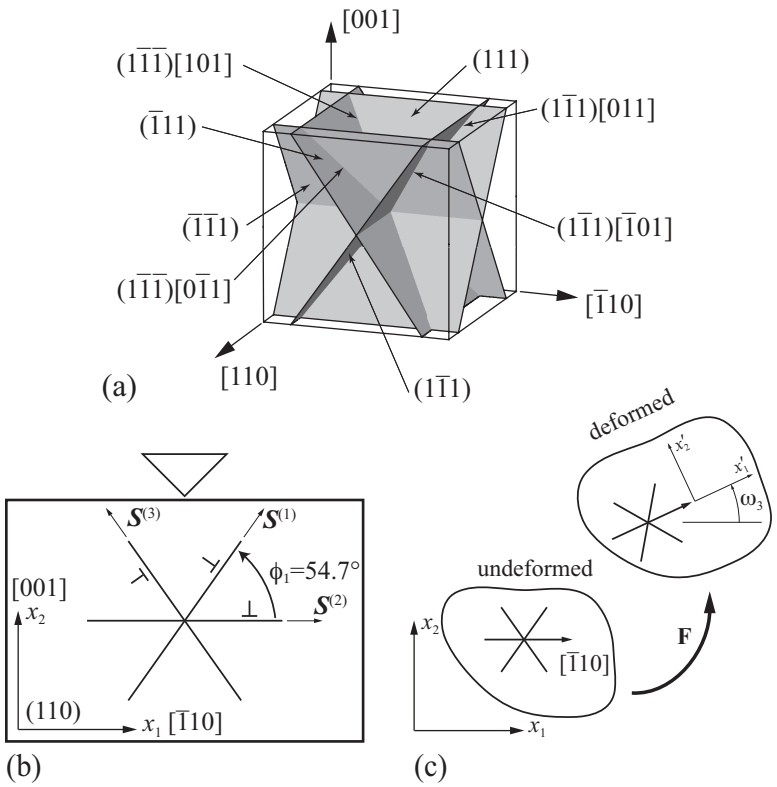

Figure 1: Crystallography of face-centered cubic crystal: a) Illustration of crystallographic slip systems relative to wire-frame specimen; b) Orientations of three effective plane strain slip systems are denoted by in-plane effective unit slip directions $\mathbf{S}^{(\alpha)}$, and the sense of a positive dislocation on each slip system is shown; c) Relationship between reference (undeformed) frame and local (deformed) frame as determined by the deformation gradient tensor $\mathbf{F}$.

is highly constrained to yield only in-plane lattice rotation, the complexity of the material response is not sacrificed.

After inducing plastic deformation via wedge indentation, the specimen was sectioned on a mid-plane by wire Electrical Discharge Machine (EDM) and polished mechanically and electrochemically. Then the spatial distribution of ω_3 was measured on the newly exposed plane in order to determine the lattice rotation field. At the outset of the project, we employed conventional Electron Backscatter Diffraction (EBSD) to measure the as-deformed lattice orientation relative to the undeformed reference configuration. In later stages of the project, we employed High Resolution Electron Backscatter Diffraction (HR-EBSD) to measure the spatial variation of ω_3. Conventional EBSD determines the absolute orientation of a crystal lattice to within $\pm 0.5^\circ$ whereas HR-EBSD determines the absolute orientation to within $\pm 0.005^\circ$ and is also capable of measuring the elastic lattice strain [2]. The two-order-of-magnitude increase in accuracy plays a decisive role in making the multiscale measurements reported herein.

It is well-known (e.g. [1]) that the Nye dislocation density tensor, α_{ij}, provides a link between the elastic deformation and the plastic deformation of the crystal. If infinitesimal

lattice rotations about the x_1-, x_2-, and x_3-axes are denoted ω_1, ω_2 and ω_3, respectively, the second-rank non-symmetric crystal lattice curvature tensor, κ_{ji}, is defined as $\kappa_{ji} = \partial\omega_j/\partial x_i$. The lattice curvature tensor is employed in the definition of the Nye dislocation density tensor as

$$\alpha_{ij} = -\kappa_{ji} + \delta_{ij}\kappa_{kk} + e_{jpk}\epsilon^{el}_{ik,p} \tag{1}$$

where δ_{ij} is the Kronecker delta, e_{ipk} is the third-rank permutation tensor, ϵ^{el}_{jk} is the elastic strain of the crystal lattice, and the comma in the subscript refers to differentiation with respect x_p. This expression is derived based upon considerations of the incompatibility of the elastic portion of the overall deformation.

In principle, all quantities on the right hand side of Eq. 1 can be measured via spatially-resolved diffractions methods. However since EBSD and HR-EBSD are limited to measurement on a surface, the out-of-plane gradients can not be accessed. This motivated the choice of specimen geometry and loading configuration in Fig. 1 for which ω_1, ω_2 as well as all out-of-plane gradients are ideally zero. Under those circumstances, the only two non-zero values of the Nye tensor are α_{13} and α_{23} which can both be measured unambiguously via HR-EBSD. (We have made measurements of the elastic strain gradient term with HR-EBSD and shown its contribution in Eq. 1 to be much smaller than the lattice curvature terms for this experimental configuration.) We made spatially-resolved HR-EBSD measurements of α_{13} and α_{23} with spatial resolutions ranging from 20 nm to 3 μm. Then we expressed the Nye tensor components in the x'_1, x'_2 crystal coordinate frame shown in Fig. 1d, and denoted the results as α'_{13} and α'_{23}.

We now consider the relationship between the Nye dislocation density tensor and the GND densities on individual slip systems. For a material with N_e active edge crystallographic slip systems and N_s active screw crystallographic slip systems, the Nye dislocation density tensor, α_{ij}, is related to the GND densities as

$$\alpha_{ij} = \sum_{\beta=1}^{N_e} \rho^{(\beta)}_{gnd(e)} b^{(\beta)} s^{(\beta)}_i t^{(\beta)}_j + \sum_{\beta=1}^{N_s} \rho^{(\beta)}_{gnd(s)} b^{(\beta)} s^{(\beta)}_i s^{(\beta)}_j \tag{2}$$

where $b^{(\beta)}$ is the Burgers vector magnitude of the β-th crystallographic slip system, $\mathbf{n}^{(\beta)}$ is the unit normal vector of the slip plane, $\mathbf{s}^{(\alpha)}$ is the unit vector in its direction of slip direction , and $\mathbf{t}^{(\beta)} = \mathbf{s}^{(\beta)} \times \mathbf{n}^{(\beta)}$ is its unit tangent vector that indicates the line sense of the dislocation line. The quantities $\rho^{(\beta)}_{gnd(e)}$ and $\rho^{(\beta)}_{gnd(s)}$ indicate the edge and screw components, respectively, of the GND densities. This expression is derived based upon considerations of the incompatibility of the plastic portion of the overall deformation.

Upon applying Eq. 2 to the experimental configuration for FCC crystals in Fig. 1, we showed that of the GND content on the three activated slip system pairs can be described uniquely by three independent edge GND densities. The relationship between the measured α'_{13} and α'_{23} and the unknown $\rho^{(1)}_{gnd(e)}$, $\rho^{(2)}_{gnd(e)}$ and $\rho^{(3)}_{gnd(e)}$ is

$$\begin{bmatrix} \alpha'_{13} \\ \alpha'_{23} \end{bmatrix} = \begin{bmatrix} +\frac{2}{\sqrt{3}} & +\frac{2}{\sqrt{3}} & -\frac{2}{\sqrt{3}} \\ +\frac{2\sqrt{2}}{\sqrt{3}} & 0 & +\frac{2\sqrt{2}}{\sqrt{3}} \end{bmatrix} \begin{bmatrix} \rho^{(1)}_{gnd(e)} b^{(1)} \\ \rho^{(2)}_{gnd(e)} b^{(2)} \\ \rho^{(3)}_{gnd(e)} b^{(3)} \end{bmatrix} \tag{3}$$

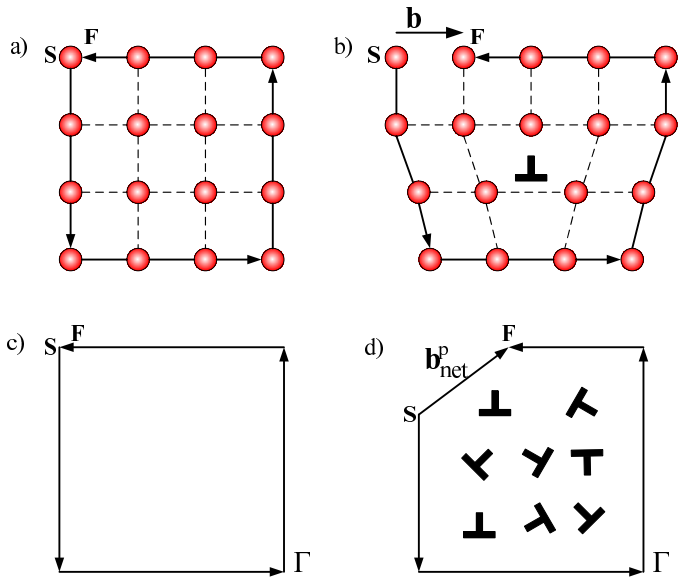

Figure 2: Crystal lattice and the Burgers circuits: (a) Crystal lattice without any dislocation; (b) Crystal lattice with a single dislocation and the Burgers vector, $\mathbf{b}$; (c) Circuit Γ on plane with unit normal $\mathbf{m}$ not cut by dislocations; (d) Burgers circuit after plane with unit normal is cut by dislocations to determine net Burgers vector, $\mathbf{b}^p_{net}$.

which is in general an underdetermined system. The total GND density is defined as $\rho^{tot}_{gnd} = \left|\rho^{(1)}_{gnd}\right| + \left|\rho^{(2)}_{gnd}\right| + \left|\rho^{(3)}_{gnd}\right|$. Upon minimizing ρ^{tot}_{gnd} subject to the constraint in Eq. 3, we found a rigorous analytical solution for the lower bound on the total GND density as detailed in [1]. It is interesting to note that in circumstances in which only one or two slip system pairs are activated, the GND densities on any unactivated slip system pair is known to be precisely zero and, hence, Eq. 3 can be solved exactly to determine unambiguously the non-zero GND densities. Under such conditions, the lower bound solution reduces to the exact solution.

In order to understand the physical significance of the Nye tensor, we consider the Burgers circuits shown in Fig. 1. If a Burgers circuit is taken on a plane with unit normal vector $\mathbf{m}$ in Fig. 1a, the Burgers vector, $\mathbf{b}$, is determined by the closure failure vector around a single dislocation in Fig. 1b. Likewise for a larger Burgers circuit denoted by Γ enclosing a scalar area A in Fig. 1c again on a plane with unit normal vector $\mathbf{m}$, the net Burgers vector, $\mathbf{b}^p_{net}$, is determined by the closure failure vector around many dislocations. The Net Burgers Density Vector is then defined as $\mathbf{B} = \mathbf{b}^p_{net}/A$ which has units of inverse length. The Net Burgers Density Vector is regularly measured by Transmission Electron Microscopy (TEM) based upon discrete measurements of dislocations.

The Net Burgers Density Vector can also be calculated as

$$\mathbf{B} = \alpha \cdot \boldsymbol{m} \tag{4}$$

where again $\mathbf{m}$ is the unit normal vector to the plane of the Burgers circuit. Thus it is seen that the Nye tensor is the continuum manifestation of a Burgers circuit in the sense that it transforms the vector $\mathbf{m}$ to $\mathbf{B}$. We use continuum methods to measure the Nye tensor based upon HR-EBSD in a Scanning Electron Microscope (SEM). Thus we see that the Nye tensor

provides a linkage between the elastic and plastic deformation in Eq. 1 and Eq. 2 as well as a linkage between a discrete and a continuum perspective of dislocations.

Multiple Length Scale Experimental Results

The lattice rotation, ω_3, associated with wedge indentation (with a 90° included angle) that impinges into a single nickel crystal is shown in Fig. 3, based upon HR-EBSD measurements. The data in the first row of Fig. 3 are obtained by sampling with a 2500 nm spatial resolution. The data in the second row are obtain by resampling with a 500 nm spatial resolution the region within the white wireframe in the first row. Likewise the data in the third row are obtain by resampling with a 100 nm spatial resolution the region within the white wireframe in the second row.

We notice several things of interest in Fig. 3. First, the GND densities have a quasi-periodic variation in crystallographically significant directions. Second, the wavelength of the quasi-periodic variation decreases as the spatial resolutions decrease. Third, the GND structures become more well-defined as the spatial resolution of the measurement decreases. At the smallest length scales in Fig. 3f, the GND structures correspond to dislocation cell structures. Hence, our methods are capable of making quantitive measurements dislocation cell structures based upon SEM measurements and continuum concepts.

A combined image of the Lower Bound on Total GND density is shown in Fig. 4 where the Net Burgers Density Vector, $\mathbf{B}$, is shown on a 100 nm by 100 nm array of deformed material points. It is clear that $\mathbf{B}$ has a larger magnitude within the dislocation cell walls.

The Lower Bound on the Total GND density can be apportioned onto the GND densities on the constituent slip system pairs according to the conventions in Fig. 1b. The black traces overlaying the plots indicate as-deformed slip directions of the respective slip system pairs. It is evident that the GND structures predominantly lie perpendicular to the as-deformed slip directions, which indicates that the GND density structures indicate the presence of dislocation walls. Furthermore, the dislocation walls are spaced quasi-periodically along the slip directions. In the regions of highest deformation where the spatial resolution is the smallest, the dislocation structures likewise can be interpreted as constituting the walls of dislocation cell structures. Hence we interpret the quasi-periodic structure of GND densities in regions of lower deformation and larger spatial resolution as being incipient dislocation cell wall structures.

This motivated us to quantify the relationship between the wavelength of the quasi-periodic GND density structures and the peak GND densities within the walls as seen in Fig. 6. The linear relationship between dislocation cell size and peak GND density in the right column is consistent with the well-known Principle of Similitude between the same variables that have been measured via TEM for many materials. Such a close correspondence between our methods and the well-established TEM methods provides a strong validation of our methods. However our results extend the Principle of Similitude by an order of magnitude greater dislocation cell structures than measured via TEM. Hence our results suggest that the Principle of Similitude is operative at the earliest stages of deformation where the dislocation cell structures are incipient.

The dislocation mean free path length must scale with the dislocation cell structure because the cell walls trap dislocations as they develop. We claim that the dislocation mean

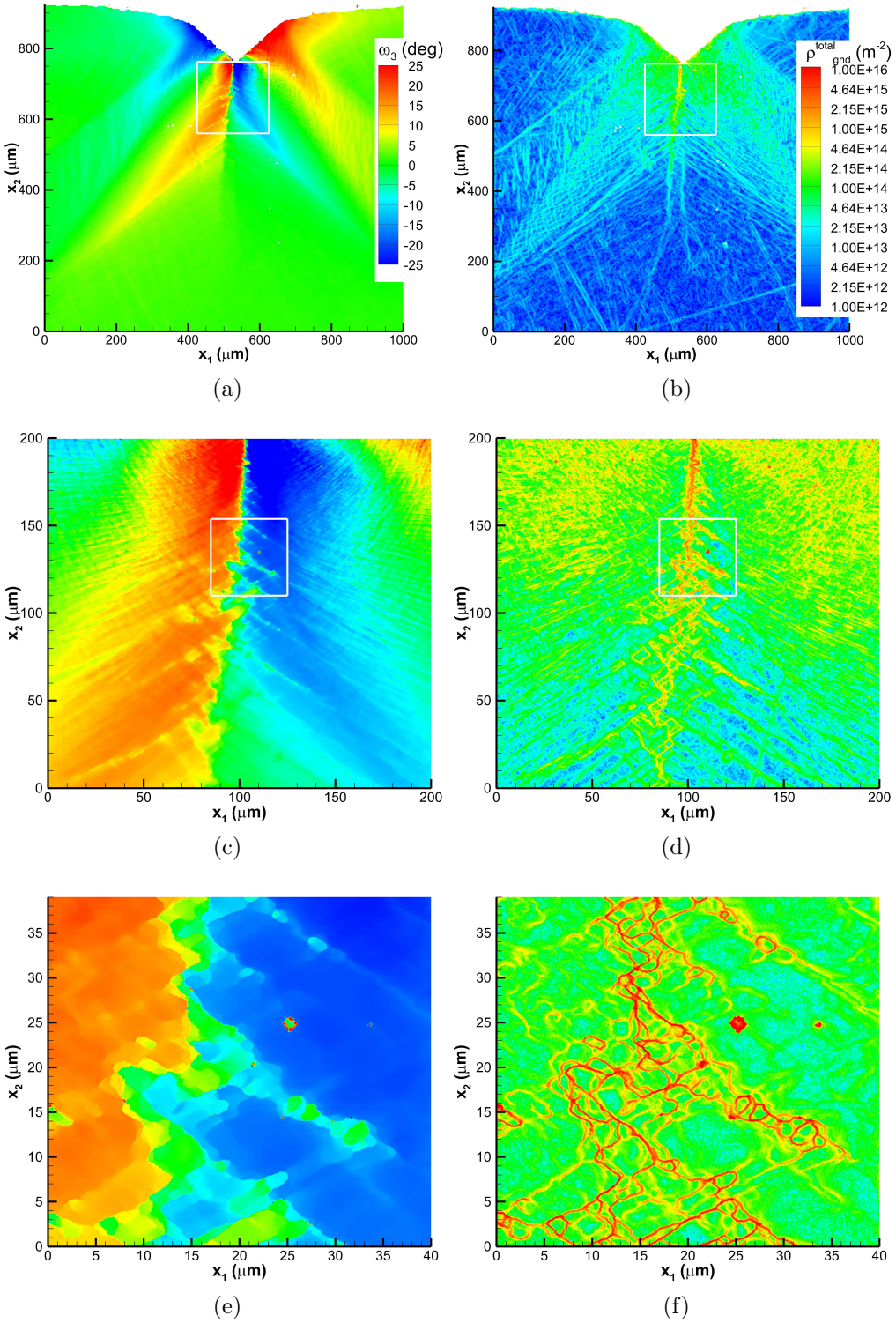

Figure 3: Multiple length scale measurements of lattice rotations, ω_3 with units of degrees in left column and corresponding Lower Bound Total GND densities with units of m^{-1} in right column with spatial resolution 2500 nm in (a–b), 500 nm in (c–d) (area bounded with the white wireframe above is resampled experimentally) and 100 nm in (e–f) (area bounded with the white wireframe above is resampled experimentally).

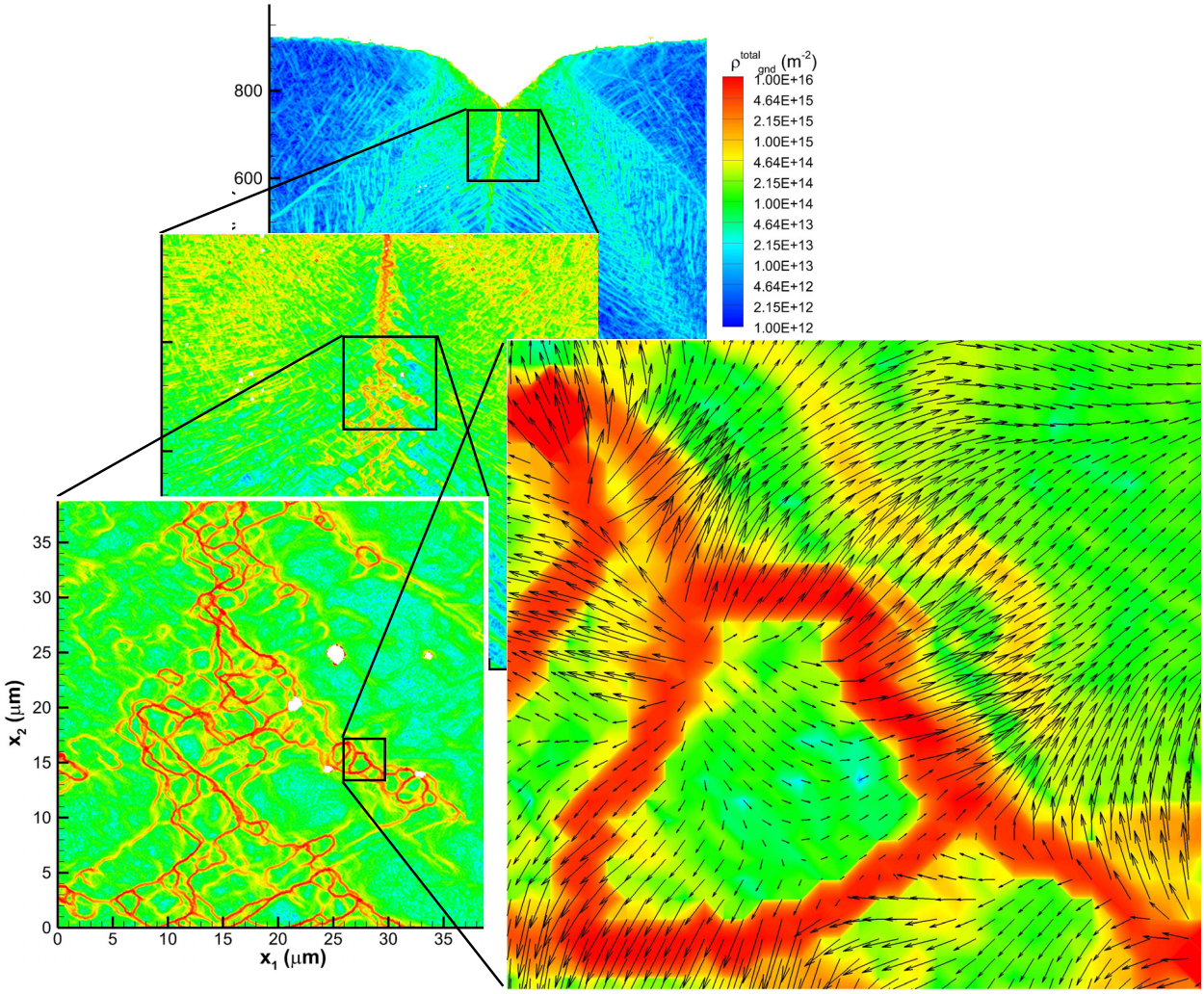

Figure 4: Multiscale perspective of Lower Bound on Total GND Density. The back three images are from the right column of Fig. 3. The Net Burgers Density Vector, $\mathbf{B}$, is shown on a 100 nm by 100 nm array of deformed material points.

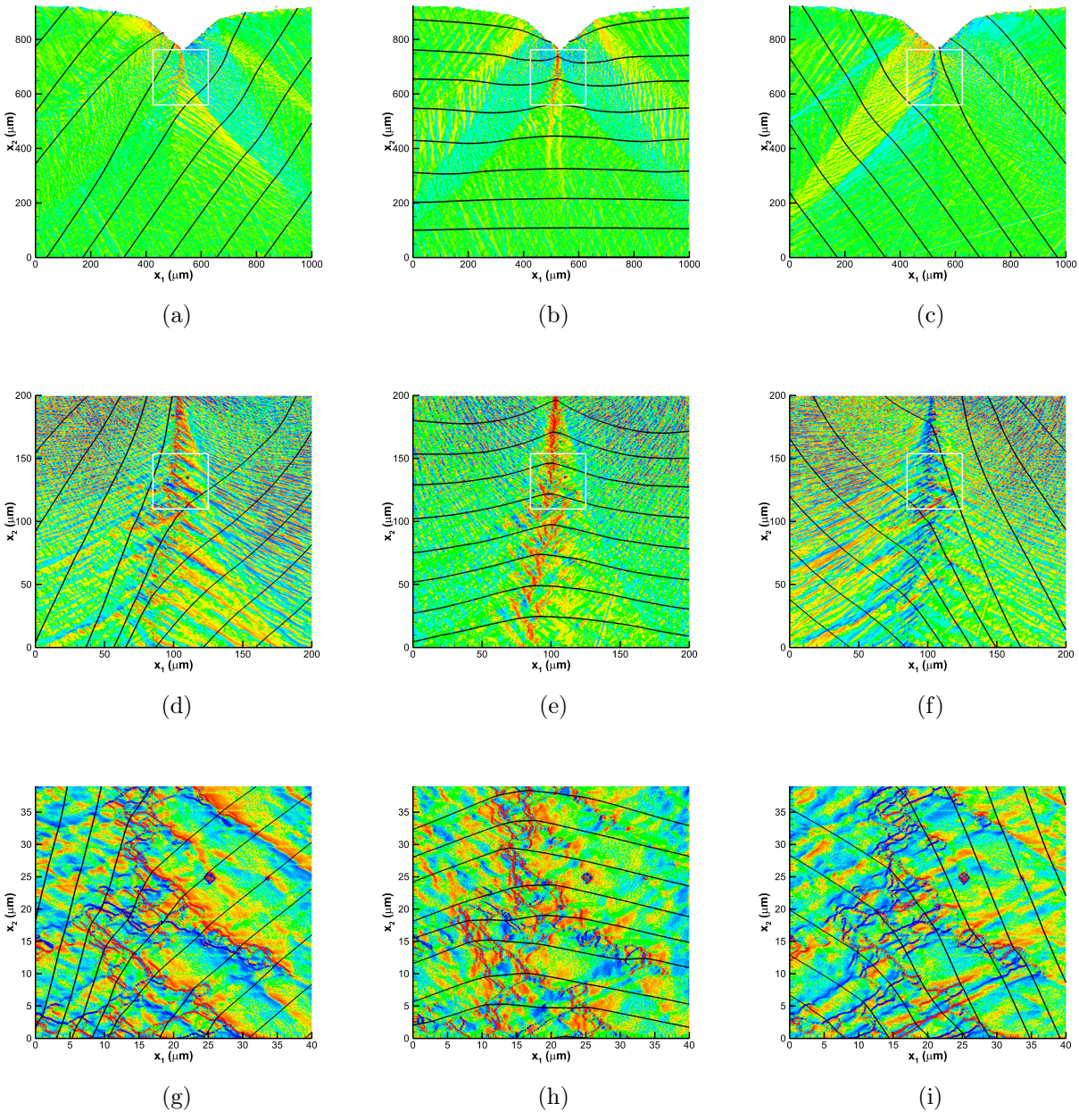

Figure 5: The three columns show GND density distributions on slip pair 1 (left column), slip pair 2 (middle column) and slip pair 3 (right column), with spatial resolutions along the rows of 2500 nm (top row), 500 nm (middle row) and 100 nm (bottom row.

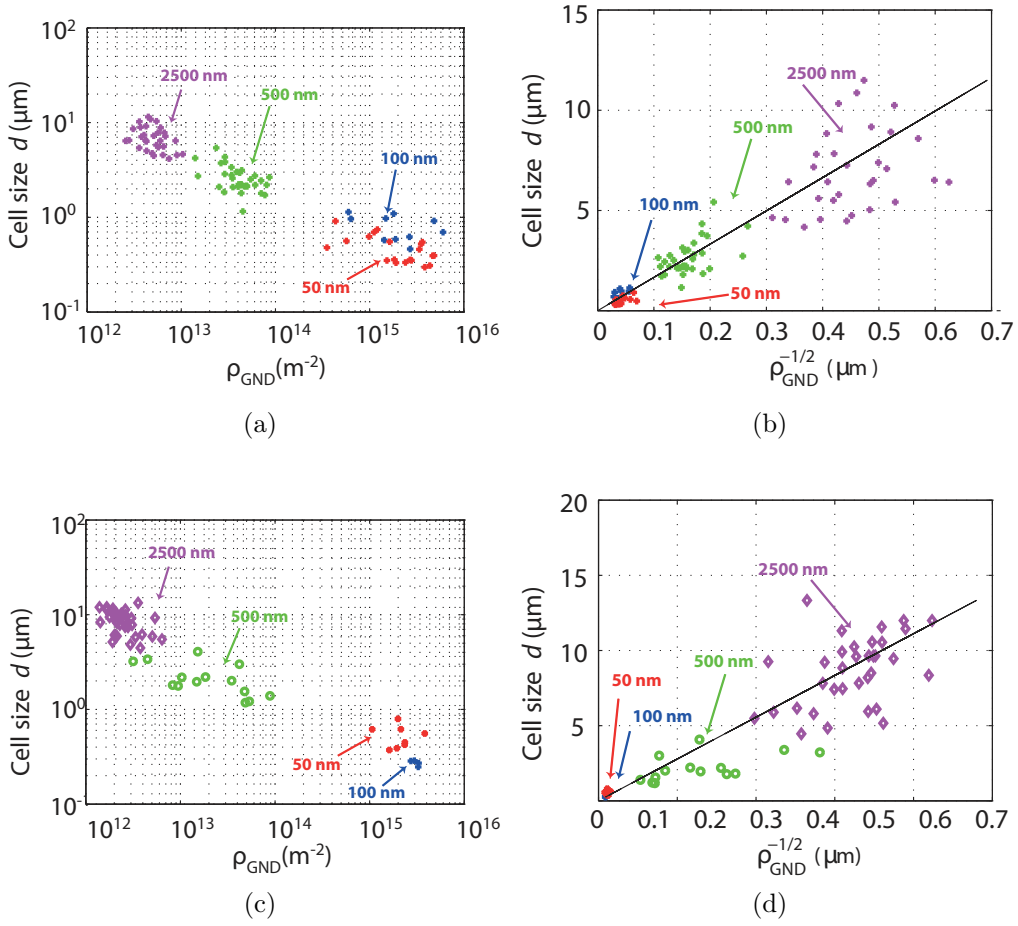

Figure 6: Dislocation cell size versus peak GND densities for different spatial resolutions in regions of simultaneous slip in slip pairs 1 and 3 shown in top row and for regions of slip solely on slip pair 2.

free path length is the intrinsic length scale of crystal plasticity. In that sense the linear fits in the right column of Fig. 6 can be interpreted as a scaling relationships for the mean free path length of dislocations. The mean free path length decreases as the peak GND density increases as a consequence of increased plastic deformation. Furthermore, the scatter of the results vertically above and below the linear relationship indicates the standard deviation of the dislocation free path length. Overall then we can interpret the intrinsic length scale of crystal plasticity: (1) as having a range rather than being a discrete value; and, (2) as evolving with increasing deformation. The results of this aspect of the project will be published [16].

The scaling relationship for the dislocation mean free path length spans across the mesoscale of plastic deformation, from the the sub-micrometer where discrete dislocation (DD) plasticity simulations are used to investigate plastic deformation up to tens of micrometer length scale where continuum dislocation (CD) plasticity simulations are often used. As such, this scaling relationship has the potential to guide both DD and CD plasticity simulations to model the behavior in both regimes, which would provide a means of spanning the mesoscale with computer simulations. To this end, we performed detailed simulations of how quasi-periodic variation of GND densities affect the hardening behavior of single crystals [11].

In addition, we performed many experiments similar experiments with body-centered cubic (BCC) tantalum. A BCC crystal can also be oriented so as to obtain a plane strain deformation state as a consequence of plastic slip on three sets of slip systems, as seen in Fig. 1. While the undeformed crystal is oriented a 90° rotation about the [110] axis from that of the undeformed FCC crystal, the three sets of slip systems that lead to the effective in-plane slip systems are oriented relative to the specimen coordinate frame precisely like the analogous sets of slip systems in the FCC crystal. Hence the analysis of the experimental results is almost identical for both cases.

After indenting a tantalum crystal under quasistatic conditions with a 90° wedge indenter, we measured the as-deformed lattice rotation about the [110] axis and determined the spatial variation of ω_3. The results of multiscale measurements are indicated in Fig. 8, with spatial resolutions of 2500 nm, 150 nm and 20 nm from left to right. The top row of the figure consist of image quality maps from the HR-EBSD measurements and the bottom row shows the in-plane lattice rotation.

Upon calculating the Lower Bound on the Total GND Density and apportioning the total GND density to the individual constituent slip system, we find the results in Fig. 9. The results have many qualitative similarities with the GND density distributions found in similarly indented FCC crystals, especially in the general spatial distribution and the appearance of quasi-periodic GND variation. One main difference is the vary rapid oscillations in lattice rotation found in the material immediately under the indenter tip, which could be a sign of twinning deformation. The results of the tantalum experiments will be published [15].

We have also plotted the angle, denoted as β, of the Net Burgers Density Vector relative to the x_1-axis. We demonstrated thatthe resulting β-field gives critical information about what sets of slip systems have been activated at a material point. In addition, we have demonstrated that the β-field is a very sensitive means of experimentally validating constitutive hardening formulations for crystal plasticity [18, 17].

Another set of experiments we have published [13] is a study in which we systematically

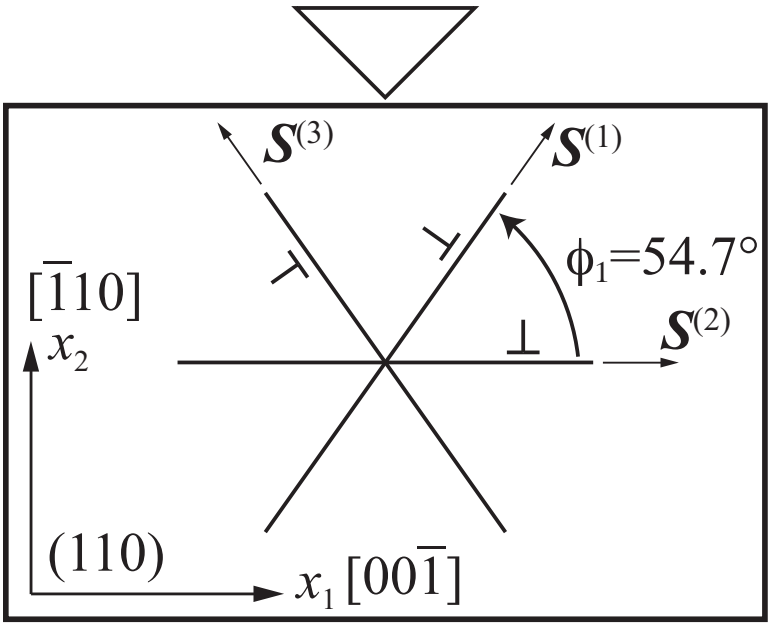

Figure 7: Crystallography of body-centered cubic crystal with orientations of three effective plane strain slip systems are denoted by in-plane effective unit slip directions $\mathbf{S}^{(\alpha)}$, and the sense of a positive dislocation on each slip system is shown.

vary the included angle of the wedge indenter while holding all other variables constant in a single nickel crystal. The results indicate that the abrupt jump in lattice rotation across the vertical mid-plane of the domain immediately beneath the indenter tip is also a sensitive means of providing experimental validation for constitutive parameters.

We published a pair of analytical and computational studies [3, 7] in which we investigated in detail the deformation field immediately under the wedge indenter tip. A detailed analytic asymptotic analysis gave insight into the form of the deformation field, which was followed up by a detailed finite element crystal plasticity analysis to investigate how far into the material the asymptotic structure propagated. The results of these studies give significant insight into how to interpret properly the GND density field.

We participated in a study led by Brent Adams of Brigham Young University in which we investigated the newly-developed method of HR-EBSD and compared it to conventional EBSD. The resulting publication [2] provides rationale for applying the HR-EBSD method to our present experiments.

We published two other studies that involved spatially-resolved measurements of GND density. One [14] was the measurement of GND densities in a bicrystal of aluminum, which gives insight into dislocation and/or slip transmission across grain boundaries. The other [4] was to characterize the GND densities in an aluminum bicrystal subject to laser shock peening.

Finally we acknowledged AFOSR for several other papers [5, 8, 6, 10, 12, 9] from the PI's laboratory throughout the course of this project because the equipment either purchased or maintained through AFOSR grants was used in those studies. One of the studies that probed the mechanical strength of polycrystalline graphene films grown by chemical vapor

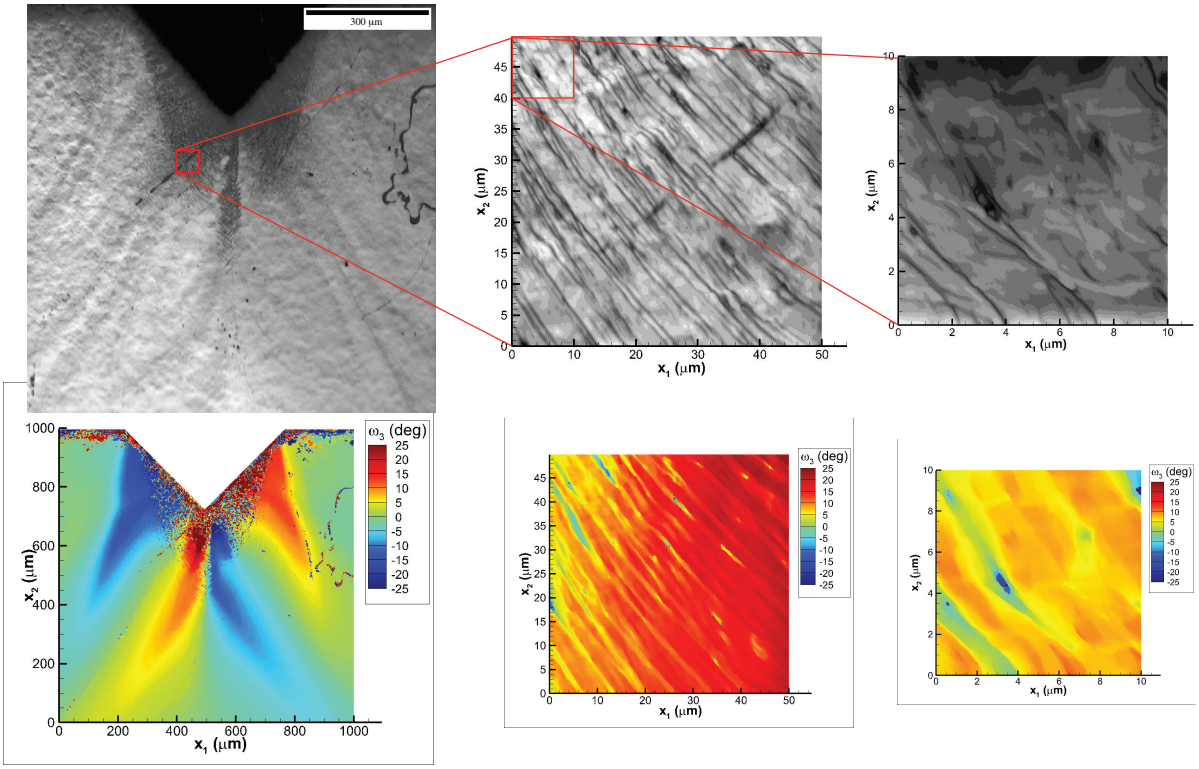

Figure 8: Crystallography of body-centered cubic crystal with orientations of three effective plane strain slip systems are denoted by in-plane effective unit slip directions $\mathbf{S}^{(\alpha)}$, and the sense of a positive dislocation on each slip system is shown.

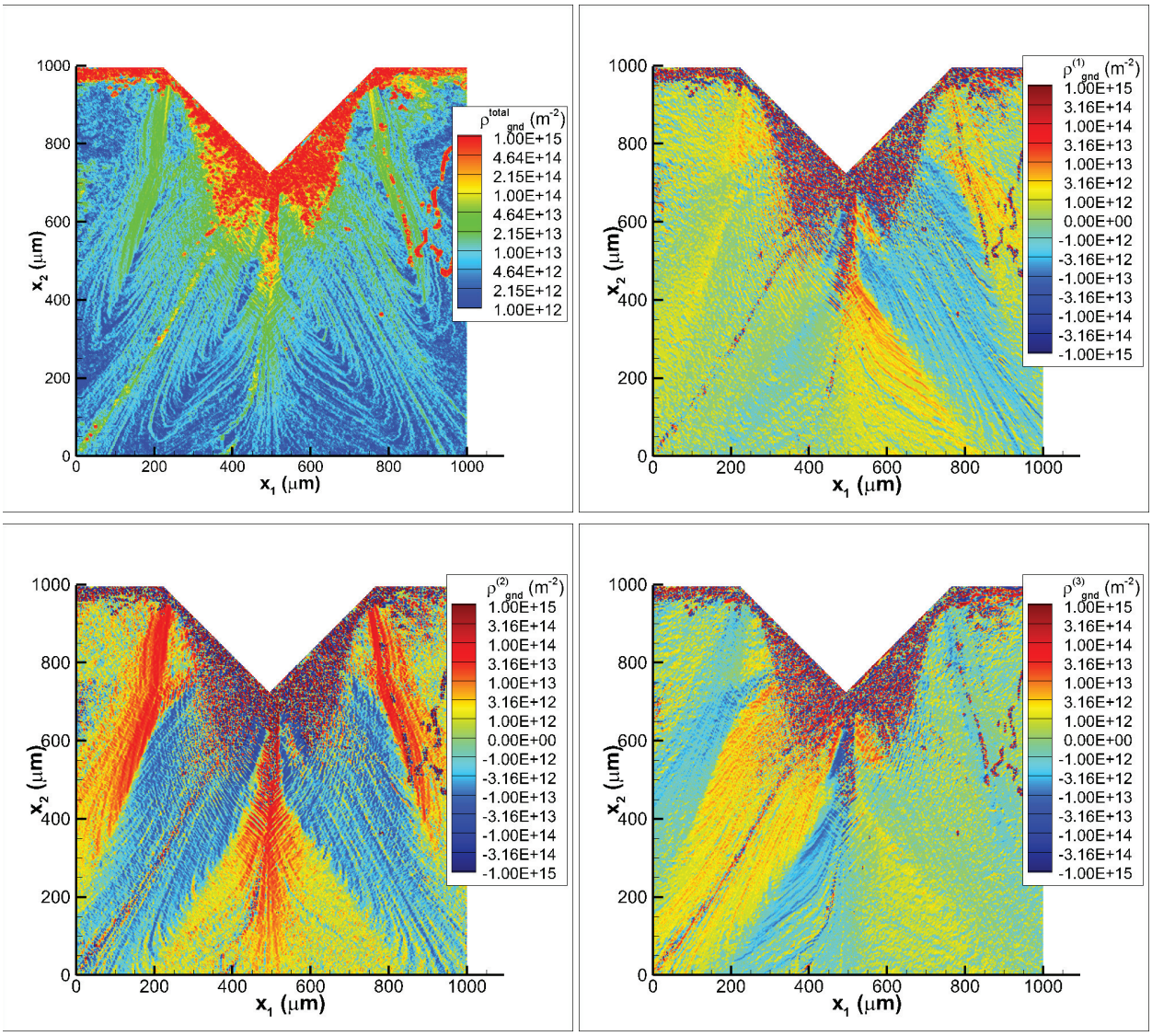

Figure 9: Lower bound GND densities with spatial resolution of 2500 nm in tantalum crystal: Upper left is total; upper right is for slip system set 1; lower left is for slip system set 2; lower right is for slip system set 3.

deposition demonstrated that such graphene can be almost as strong as pristine defect-free graphene, which itself is the strongest known material. This study was published in *Science* [10]. Another paper that deals with graphene-metal composites appeared in *Nature Communications* [9].

Archival publications during reporting period:

[1] J. W. Kysar, Y. Saito, M. S. Öztop, D. Lee, and W. T. Huh. Experimental lower bounds on geometrically necessary dislocation density. *International Journal of Plasticity*, 26(8):1097–1123, 2010.

[2] C. J. Gardner, J. Kacher, J. Basinger, B. L. Adams, M. S. Öztop, and J. W. Kysar. Techniques and applications of the simulated pattern adaptation of Wilkinson's method for advanced microstructure analysis. *Experimental Mechanics*, 51(8):1379–1393, 2011.

[3] Y. Saito and J. W. Kysar. Wedge indentation into elastic-plastic single crystals, 1: Asymptotic fields for nearly-flat wedge. *International Journal of Plasticity*, 27(10):1640–1657, 2011.

[4] S. Vukelić, I. C. Noyan, J. W. Kysar, and Y. L. Yao. Characterization of heterogeneous response of Al bicrystal subject to micro scale laser shock peening. *Experimental Mechanics*, 51(5):793–796, 2011.

[5] X. Wei and J. W. Kysar. Residual plastic strain recovery driven by grain-boundary diffusion in nanocrystalline thin films. *Acta Materialia*, 59(10):3937–3945, 2011.

[6] O. Gaathon, J. D. Adam, S. V. Krishnaswamy, J. W. Kysar, S. Bakhru, K. Bakhru, D. O. Welch, and R. M. Osgood Jr. Planar single-crystal thin-films of YAG obtained by ion implantation and thermal exfoliation. *Optical Materials*, 35(1):25–28, 2012.

[7] Y. Saito, M. S. Öztop, and J. W. Kysar. Wedge indentation into elastic-plastic single crystals, 2: Simulations for face-centered cubic crystals. *International Journal of Plasticity*, 28(1):70–87, 2012.

[8] X. Wei and J. W. Kysar. Experimental validation of multiscale modeling of indentation of suspended circular graphene membranes. *International Journal of Solids and Structures*, 49(22):3201–3209, 2012.

[9] Y. Kim, J. Lee, M. S. Yeom, J. W. Shin, H. Kim, Y. Cui, J. W. Kysar, J. Hone, Y. Jung, S. Jeon, and S. M. Han. Strengthening effect of single-atomic-layer graphene in metal–graphene nanolayered composites. *Nature Communications*, 4:2114, 2013.

[10] G.-H. Lee, R. C. Cooper, S. J. An, S. Lee, A. van der Zande, N. Petrone, A. G. Hammerberg, C. Lee, B. Crawford, W. Oliver, J. W. Kysar, and J. Hone. High-Strength Chemical-Vapor–Deposited Graphene and Grain Boundaries. *Science*, 340(6136):1073–1076, 2013.

[11] M. S. Öztop, J. W. Kysar, and C. F. Niordson. Length-scale effect due to periodic variation of geometrically necessary dislocation densities. *International Journal of Plasticity*, 41(1):189–201, 2013.

[12] M. Yilmaz and J. W. Kysar. Monolithic integration of nanoscale tensile specimens and MEMS structures. *Nanotechnology*, 24(16):165502, 2013.

[13] C. F. O. Dahlberg, Y. Saito, M. S. Öztop, and J. W. Kysar. Geometrically necessary dislocation density measurements associated with different angles of indentations. *International Journal of Plasticity*, 54(1):81–95, 2014.

[14] M. S. Öztop, A. L. Ekberg, C. F. O. Dahlberg, and J. W. Kysar. Geometrically necessary dislocation density measurements associated with wedge indentation into an aluminum bicrystal. To be submitted, 2014.

[15] M. S. Öztop, A. L. Ekberg, C. F. O. Dahlberg, and J. W. Kysar. Multiple length scale measurements of geometrically necessary dislocation (GND) densities in tantalum. *Journal of Materials Research*, To be submitted, 2014.

[16] M. S. Öztop, C. J. Gardner, C. F. Niordson, C. F. O. Dahlberg, B. L. Adams, and J. W. Kysar. Intrinsic length scale and its evolution in crystal plasticity. To be submitted, 2014.

[17] A. Sarac, M. S. Öztop, C. F. O. Dahlberg, and J. W. Kysar. Net Burgers vector density fields spatial distribution: Constitutive model validation. To be submitted, 2014.

[18] A. Sarac, M. S. Öztop, C. F. O. Dahlberg, and J. W. Kysar. Net Burgers vector density fields spatial distribution: Experimental measurements. To be submitted, 2014.

List of Awards and Honors:

- Best Poster Award, Joint National Synchrotron Light Source and Center for Functional Nanomaterials Users' Meeting at Brookhaven National Laboratory 2012
- International Journal of Plasticity Young Researcher Award 2012
- "Hot Paper in Chemistry" as reported by Science Watch during March-June 2010 as "the most-cited chemistry report published in the last two years, excluding reviews" 2010

List of Synergistic Activities

- Organizing or Scientific Committees for Conferences
  - Fourth Biot Conference, New York City 2009
  - International Symposium on Plasticity, Nassau, Bahamas 2013
  - International Symposium on Plasticity, Freeport, Bahamas 2014

  - International Workshop on Computational Mechanics of Materials, Spain . . 2014

- Symposia Organization
  - Organized symposia at American Society of Mechanical Engineers (ASME) annual International Mechanical Engineering Congress and Exposition (IMECE) . 2002–2014
  - Organized mini-symposium at the International Symposium on Plasticity . 2013–2014

- Editorial Responsibilities
  - Editorial Board Member *International Journal of Solids and Structures* . . . 2013–present
  - Regional Editor *International Journal of Fracture* 2013–present
  - Editorial Advisory Board *International Journal of Plasticity* 2007–present
  - Associate Editor *Journal of Engineering Materials and Technology* . . . 2010–2013
  - Associate Technical Editor *Experimental Mechanics* 2007–2013
  - Editorial Advisory Board *The Open Mechanical Engineering Journal* . 2007–2009